NASA-CR-200982

PROJECT CLOSING REPORT

MICROSTRUCTURAL AND MICROCHEMICAL

CHARACTERIZATION OF

ELEVATED TEMPERATURE MATERIALS

(NCC-3-111, TWIR-5)

Submitted to:

NASA-Lewis Research Center

Cleveland, OH 44135

Aircraft gas-turbine engine requirements have traditionally lead the pace of development of elevated temperature materials. Increasing engine efficiency and performance capabilities have been obtained for gas turbine components, such as, blades, vanes and disks, by clever materials and processing developments. Knowledge and understanding of processing-microstructure and mechanical properties relationships have been critical in these developments. The operating temperatures of superalloys have, however, now been pushed close to their incipient melting points. It is generally believed that further significant improvements in temperature capability can be obtained only by using the intermetallics, ceramics or refractory elements. These, however, are inherently brittle, at least at the room temperature. Effect of minor alloying additions (such as, boron, yttrium, in NI_3Al) and innovative processing techniques (such as, rapid solidification, plasma processing) are being extensively investigated to overcome this major problem of alloy ductility.

WORK PERFORMED: Under this cooperative agreement X-ray diffraction analysis related support was provided for the high temperature materials research and development programs in the Materials Division. Ruth Cipcic was also involved with improving the X-ray diffraction analysis capability within the division, besides her direct research involvement.

(1) **High temperature X-ray diffraction:** The heating control (introduction of two DC power sources) and software (to incorporate Scintag's High Temperature Program) were modified to obtain better temperature control across the strip heater. The system was also

modified to provide controlled gaseous atmosphere for oxidation and other related studies. The heating control (introduction of two DC power sources) and software (to incorporate Scintag's High Temperature Program) were tested and improved to obtain better temperature control across the strip heater. The high temperature X-ray diffraction capability of the system was documented. This helped identify potentially useful high temperature materials.

(2) Lauve Analysis: The routine support for the Debye-Scherrer analysis of the coated SCS-6 fibers, and texture analysis of the single crystal zirconia fibers was provided through out the duration of this project. In addition, one track, goniometer, laser mount, target and accessories were procured and installed. A laser power source was procured and used for the optical orientation during Lauve Analysis. A light box, sonic digitizer, and software were also purchased and installed for the computer capture and processing of Lauve film intensity data for cubic and hexagonal single crystals. The Lauve Analysis technique was extensively utilized after installation of the goniometer, laser mount, target and accessories. The light box, sonic digitizer, and software were used for the analysis of single crystal orientation of superalloys and intermetallic monolithic and composite materials.

Single crystals of cubic zirconia fibers were oriented in various orientations to support the fiber growth programs for the intermetallic and ceramic matrix composites for the advanced gas turbine materials applications.

The coatings on the SCS-6 fibers were analyzed by Debye Scherrer films to obtain the structural and orientation relationships.

(2) **Scanning Electron Microscopy**: Bulk of Patricia Dickerson's effort was concerned with the characterization of ceramic fibers and fiber coatings. The fibers were of a variety of compositions-single crystal sapphire, single crystal yttria stabilized zirconia, mullite, directionally solidified alumina-yag eutectic, and directionally solidified alumina-zirconia eutectics. These data were used in the HIGHTEMP 1993 and TMS Materials Week 1993

presentations. The Enabling Propulsion Materials program within the Materials Division was mostly supported by characterizing the fiber damage and compliant layer coatings on the ceramic fibers. The alumina-Nicalon fiber composites, produced by Lanxide Corporation, were also studied, subsequent to the boron nitride and CVD silicon carbide coatings. Small impurities on the fiber surface related to the processing were identified. Microstructural and microchemical characterization of the directionally solidified alumina-YAG and alumina-zirconia eutectic fibers grown commercially by edge defined film fed growth techniques, and also by the laser heated floating zone method was carried out. Mulite and yttria stabilized zirconia fibers grown by laser float zone technique were examined in order to improve their processing conditions. Chromia and zirconia doped sapphire fibers were also examined in support of the metal and intermetallic matrix composite materials research in the Materials Division at the NASA-Lewis Research Center.

As and when required by the ongoing research programs in the Materials Division, a range of other high temperature materials were examined to understand the effect of microstructure on their deformation and fracture behavior. Metallic, Ceramic and composite specimens tested for a range of mechanical property requirements, such as, stress-rupture, creep, low cycle fatigue, high cycle fatigue, thermomechanical fatigue, etc, were evaluated by Scanning Electron Microscopy. The microstructural and microchemical stability of these materials exposed to simulated operating environments were examined.

(3) **Melt infiltrated composites:** Two types of melt infiltration processing, one driven mainly by surface tension of the liquid with the solid preform (for example silicon melt infiltration of porous graphite) and the other driven by application of high hydrostatic pressure (high pressure infiltration of metallic melts into the particulate or fibrous ceramic preforms), were studied in the chemical engineering department at Cleveland State University. These processing technologies were of interest to several other research programs in the materials division, for example high

thermal conductivity rocket engines (melt infiltrated copper-graphite composite), intermetallic matrix composites, etc. The silicon infiltrated graphite specimens and superalloy infiltrated sapphire (or alumina tow fibers) composite specimens processed at CSU were characterized for their microstructural and microchemical properties in order to quantitatively identify the role of critical processing steps and their influence on the composite integrity. In collaboration with Dr. Jorge Gatica, Assistant Professor, Chemical Engineering Department, numerical model of the pressure infiltration kinetics during unidirectional melt infiltration through porous preforms was carried out.

DYNAMIC ANALYSIS OF PRESSURE INFILTRATION PROCESSES

Dhiman K. Biswas, Jorge E. Gatica and Surendra N. Tewari
Department of Chemical Engineering - 455 Stilwell Hall - 1960 E. 24th Street,
Cleveland State University, Cleveland, OH 44115 (FAX: 216 / 687-9220).

ABSTRACT

Unidirectional pressure infiltration of porous preforms by molten metal/alloys is investigated in this study. The dynamics of the process is analyzed via the numerical solution of a mathematical model. Comparison against classical asymptotic analyses shows that, for realistic samples, end effects may become important and render asymptotic results unreliable. A comparison with experiments proves the model to be an efficient predictive tool in the analysis of infiltration processes for different preform/melt systems.

INTRODUCTION

For the pressure infiltration process, porous preforms are normally prepared by packing paricles/whiskers or as microporous structures (cf. Fig. 1). A superheated molten metal/alloy is then infiltrated into the preform by applying an external pressure gradient. The pressure gradient, velocity of propagation, and temperature of the preform and superheated melt; are critical variables determining the infiltration kinetics and microstructure of the final composite. Before solidification is observed, the preform permeability is constant and the infiltration velocity is only a weak function of the infiltration length. As solidification starts, a two-phase region emerges with a time-space variable solid fraction and the infiltration dynamics becomes strongly dependent on the infiltration length and solid fraction. This two-phase zone is confined between two sharp fronts; a remelting front at the point where the superheated metal enters the two-phase zone and an infiltration front. These two fronts have independent dynamics resulting in a two-phase zone which expands with the infiltration time. Because of its considerable engineering relevance to MMC fabrication, the infiltration process has been studied by several authors, from both theoretical and experimental

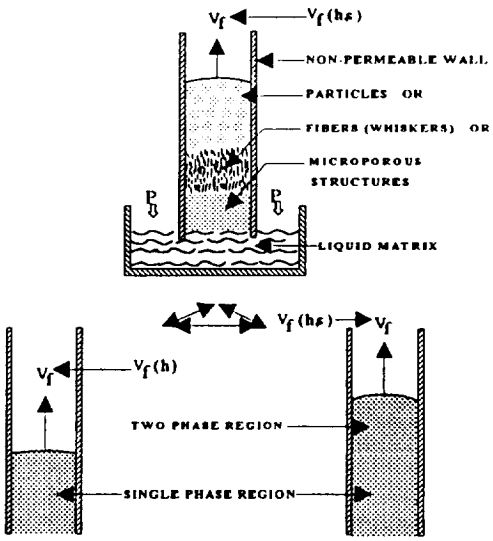

Figure 1: Schematic of the Pressure Infiltration

standpoints. Nagata and Matsuda (1982) investigated the infiltration of beds of particles ranging in size from 37 to 3400 μm. These authors proposed the existence of a critical preheating temperature, based upon physical constants of the metal and particles, above which the particles must be heated in order for infiltration to occur. Mortensen et al. (1989) investigated the critical pressure necessary for melt infiltration, and the effect of infiltration pressure on fiber perform deformation. Girot et al. (1990) performed a numerical analysis of the infiltration of liquid alloys into fibrous preforms, and proposed that flow ceases when the metal cools to its liquidus temperature and, therefore, did not account for the release of latent heat of solidification by the metal in their calculations. In this study, all these variables are investigated separately.

MODEL EQUATIONS AND ASSUMPTIONS

For analysis of fluid flow and heat transfer, a volumetric element ΔV is considered. The flow velocity through ΔV is assumed within the range of validity of Darcy's law. The dimensionless form of the momentum equation is:

$$V + \frac{\partial P}{\partial X} + Ra\theta\check{z} = 0 \qquad \text{with,} \quad \frac{\partial P}{\partial X} \approx -\frac{\Delta P}{X_f} \tag{1}$$

where, $Ra = \frac{K}{\mu}\left(\frac{\rho_c c p_c}{k_c}\right) L \rho_{mo} g(-\beta)\frac{\Delta H_m}{c p_c}$ is the Rayleigh number, $\beta = -\frac{1}{\rho_{mo}}\left|\frac{\partial \rho}{\partial T}\right|_{T_m}$ is the thermal expansion parameter, V is the dimensionless velocity, L is the total preform length, X_f is dimensionless infiltration front position, ΔP is the pressure drop in melt, and K is the preform permeability. In developing the above equation, stationary solid and fiber phases were assumed stationary, and the difference between solid and liquid metal densities was assumed negligible, i.e. the momentum transfer due to phase change is negligible. The pressure drop was assumed independent of the infiltration front velocity, and the applied pressure is considered high enough for the flow to be a slug-type flow.

The dimensionless forms of energy balance equations in the melt/composite and preform are:

$$\frac{\partial \Phi_c}{\partial t} + V\frac{\partial \Phi_m}{\partial X} = \hat{\rho}_c \frac{\partial}{\partial X}\left(\frac{\partial \theta}{\partial X}\right) + S \tag{2}$$

$$\frac{\partial \Phi_p}{\partial t} + V\frac{\partial \Phi_g}{\partial X} = \hat{\rho}_p \frac{\partial}{\partial X}\left(\frac{\partial \theta}{\partial X}\right) + S \tag{3}$$

where $\hat{\rho} = \frac{\rho}{\rho_m}$, ρ is density, Φ is the dimensionless enthalpy, θ is the dimensionless temperature and S is a source term (or energy generation in the system); the subscripts "c", "m", "p" and "g" refer to composite, matrix, preform and gas respectively. The time for heat exchange between the fibers and the metal is very short when compared to the infiltration characteristic time. Viscous heat dissipation, compression work, and volumetric energy and species sources are neglected. The interface between solid and liquid metal is assumed at thermal equilibrium, and the effect of curvature on the melting point of metal, T_m, is considered negligible.

To solve equations [1] and [2] (or [3]) simultaneously, one initial condition and three (or four) boundary conditions are necessary. The temperature in the melt and preform zone is assumed a continuous function; therefore to avoid a temperature discontinuity, the initial temperature

distribution in the preform zone is found from the analytical solution of the energy balance equation in the preform zone, i.e.

$$\theta_p(t,X) = (\theta_o - \theta_p)erfc\left[\frac{X}{C\Delta X}\right] + \theta_p \; ; \quad @\, t = 0 \qquad [4]$$

where θ_p and θ_o are the preform and melt initial temperatures, respectively.

Two of the boundary conditions can be formulated at the two interfaces. The ***infiltration front interface,*** which separates uninfiltrated preform from infiltrated two phase zone, and at the ***remelting front interface,*** which separates two phase zone from remelted single phase zone. Thermal equilibrium at the infiltration front interface establishes:

$$\vec{n}_f v_f [C_{pf} V_f \rho_f (T_m - T_f) + (-\Delta H_m)(1 - V_f)\varepsilon_s \rho_s] = \underbrace{\vec{n}_f k_p \vec{\nabla} T_p}_{very\ small} - \overbrace{\vec{n}_f k_m \vec{\nabla} T_m}^{zero(pure\ metal)} \qquad [5]$$

where, T_m is the melting temperature of the metal, v_f is front velocity, V_f is the volume fraction of fiber, ε_s is the fraction of the melt that is solidified, ΔH_m is heat of fusion of the melt, and n is the surface normal unit vector. The equilibrium condition at the remelting front interface is:

$$\vec{n}_b\left(-k_m \vec{\nabla} T_m\right) + \overbrace{\vec{n}_b\left(k_c \vec{\nabla} T_c\right)}^{zero(pure\ metal)} = (1 - V_f)\varepsilon_s(\Delta H_m)\rho_s \vec{n}_b \vec{V}_b + \underbrace{c_{pf} v_f \rho_f \left(\tilde{T}_f - T_m\right)\vec{n}_b \vec{V}_b}_{very\ small} \qquad [6]$$

where, $\tilde{T}_f$ is the fiber temperature after remelting all solid, and V_b is the bottom, remelting, front velocity. The remaining two boundary conditions, inlet and exit conditions, are assumed as suggested by Danckwerts (1953) for flow systems .

For flow perpendicular to the fiber axes, the permeability based on the numerical calculations of Sangani and Acrivos(1982) is given as:

$$K = \frac{2\sqrt{2}\, r_{sf}^2}{9 V_{sf}}\left[1 - \sqrt{\frac{4V_{sf}}{\pi}}\right]^{\frac{5}{2}} \qquad [7]$$

where, r_{sf} is the radius of the solid material and V_{sf} is its volume fraction. Eq. [7] is valid for solid volume fractions, V_{sf}, ranging between 0.2 and $\pi/4$.

SOLUTION PROCEDURE

To solve the system of differential equations [1] [2] and [3], the system is discretized, with the maximum number of cells limited by the hypothesis of continuum. The governing equations are applied for each cell, with upstream discretization for first order derivatives and central difference for second order derivatives being used. The results for temperature and enthalpy are updated after each iteration, while the solid fraction and infiltration velocity are updated only after filling each computational cell. The numerical stability is ensured by selecting the proper number of steps to "fill" a cell. The discretized equations are used directly both in the preform and melt section for each cell, except for the cell where the infiltration front is located. Incoming and outgoing fluid for the convection term for the cell where the front is, are melt and gas respectively. The heat conduction takes place on one side of this cell through the composite (fiber and melt) and on other side through the preform (fiber and gas). Therefore, the rate of energy exchange by conduction at the "front" cell is obtained by one-sided differences, which are used to find the thermal gradient for each side. Different thermal conductivities are used for each side.

RESULTS AND DISCUSSION

Typical results are presented in Figure 2, this figure shows a time sequence of thermal profiles for the infiltration of pure aluminum in an array of fibers preheated to 200 K below the metal melting temperature. It can be seen how the two-phase zone develops as soon as the melt reaches the melting temperature. Two regions can be clearly distinguished ahead and behind the infiltration front (cf. Fig. 2a), which is indicated by the steep temperature drop at the front-preform interface. As time progresses the two-phase region expands with the two fronts (remelting and infiltration, cf. Fig. 2b) exhibiting independent dynamics. At the beginning of the process the infiltration is very fast. As solidification takes place the two-phase zone permeability decreases and the infiltration is slowed down significantly. It is interesting to note that the infiltration rate determining zone is neither at the remelting or infiltration fronts, but in the bulk of the two-phase zone where the solid fraction reaches a maximum (cf. Fig 2c).

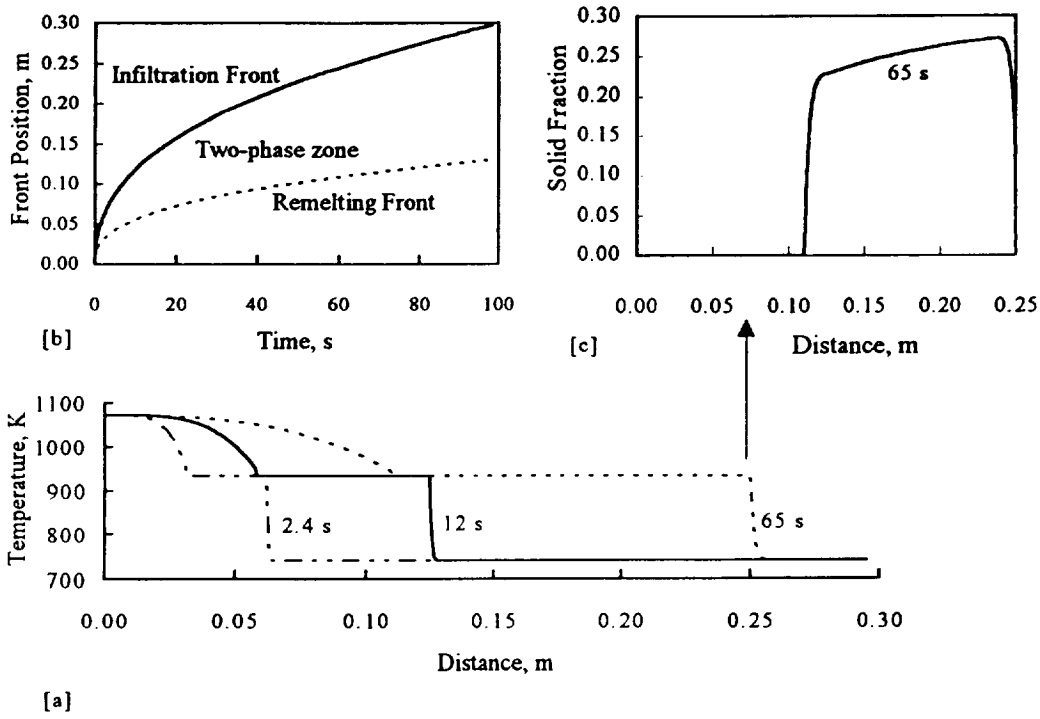

Figure 2: Infiltration dynamics for Aluminum infiltration of a fibrous preform.

When the initial fiber temperature, T_f, is sufficiently high (or when infiltration velocity is high), no solidification of the matrix occurs. The permeability in the composite is constant everywhere. This simple case is considered first to compare with the analytical model presented by Mortensen et al. (1989). The analytical and numerical results of the infiltration length as a function of time are compared (cf. Fig 3a). Satisfactory agreement between the numerical and analytical prediction validates the numerical model.

Numerical predictions can also be compared with experimental and analytical results for unidirectional adiabatic infiltration with solidification. When the initial fiber preform temperature, T_f, and the initial metal temperature (or the infiltration velocity) are sufficiently low to avoid solidification, solid metal forms at the infiltration front as a coating surrounding the packing fibers. The analytical treatment of the governing equations (Mortensen et al., 1989) solves the problem in terms of the similarity variable, $\Psi = L/\sqrt{t}$. For instance, for the conditions of Fig. 3b, the similarity variable, Ψ, for the analytical model was found to be 0.0299 m/s$^{1/2}$. For the same conditions, this parameter was found experimentally as 0.0304. This indicates a satisfactory agreement between the analytical model and the experimental results. When the analytical results are compared with the numerical model (cf. Fig 3b) some discrepancies are noticeable. These discrepancies can be explained as follows: to find the parameter, Ψ, Mortensen et al. (1989) measured the slopes of plots of the experimental infiltration length as a function of square root of the infiltration time. Since the plots were non-linear, the parameter Ψ was determined from a selected section of the plot (arbitrarily defined as that corresponding to "before sufficient solidification occurred"). The agreement between the analytical predictions and experiments, therefore, corresponds only to a portion of the experimental results, not to the entire infiltration process. A similar plot is produced in Figure 3c with the results from the numerical simulation; the numerical results are clearly consistent with the experimental observations. Indeed, the plot in Figure 3c is not linear, which is the basis for similarity solution and the main reason for disagreement between analytical and numerical results.

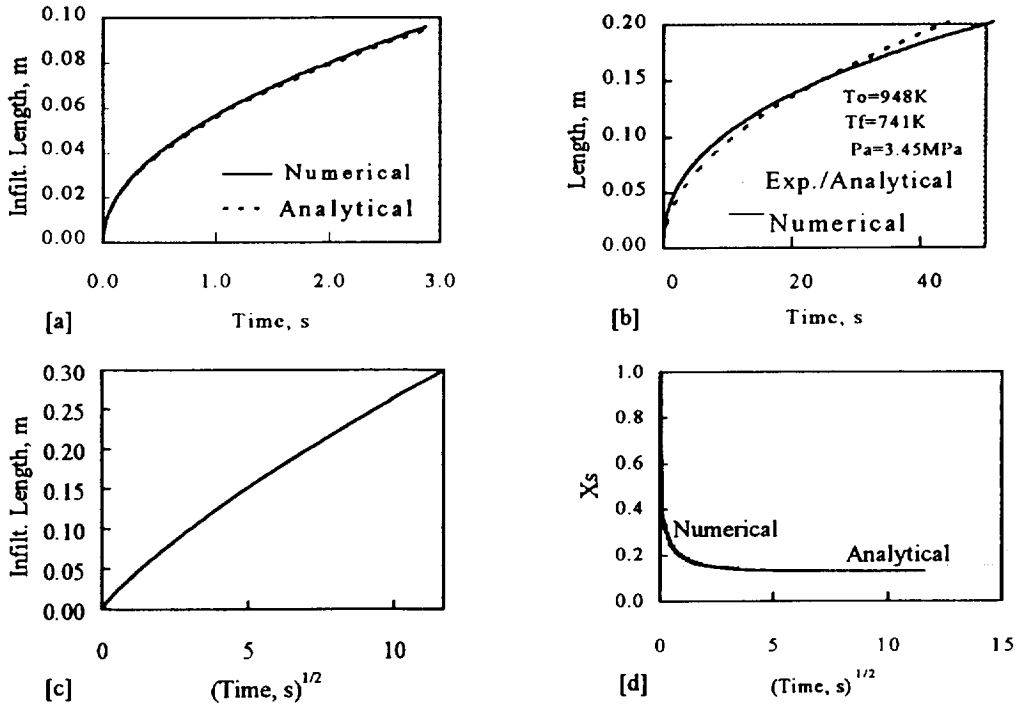

Figure 3: Comparison between numerical and experimental/analytical results.

In the analytical model, Xs, the ratio of the remelting front position to the infiltration front position, is assumed constant for given process conditions. This assumption assumes a constant-pattern propagation during the infiltration process. The parameter Xs was investigated numerically for different preform temperatures. Results for the experimental conditions reported by Masur et al. (1989) are shown in Figure 3d. The plot shows that, at beginning, the value of Xs is 1.0, i.e., the remelting and the infiltration fronts are at the same position, (i.e. the initial condition). As the melt infiltrates and solidification starts, a two-phase zone emerges and starts spreading, i.e., the value of Xs decreases and approaches an asymptotic value. The plot shows that, the value of Xs will coincide with the analytical value at about 4 seconds into the infiltration process, before this the two-phase zone is shorter and after this it is longer than the analytical value. For these experimental conditions, the analytically predicted Xs is 0.163, while numerically it was found that Xs approaches a constant value of about 0.14 after 25 seconds. Therefore, using a constant value of 0.163 for Xs, the value of the overall permeability is underestimated for the first 4 seconds of infiltration. While, after 25 seconds, the overall permeability is overestimated in the analytical model. Therefore, the prediction of the infiltration rate by the analytical model will be underestimated at the beginning, and overestimated at the end of the infiltration process. The impact on the predictive ability will depend, therefore, on the dimensions of the preform being infiltrated. For instance, Mortensen et al. (1989) presented comparisons for infiltration lengths in the range of 4-5 cm which would occur in the first 2-3 seconds of infiltration.

CONCLUSIONS

The numerical analysis presented above leads to the following conclusions :

- Actual infiltration processes never show constant pattern propagation (initial and final dynamics cannot be neglected.
- Conduction in the preform zone cannot be neglected. Although it might be negligible in determining the temperature profile.
- The two phase zone dynamics is very sensitive to the initial preform temperature.
- Asymptotic analyses can only be used as an indicative tool; not as a design tool.

ACKNOWLEDGMENTS

Support provided by the Processing Science and Technology Branch at the NASA Lewis Research Center (Cleveland, OH) is gratefully acknowledged.

REFERENCES

Danckwerts, P.V. *Chem. Eng. Sci.*, 2(1), pp. 1-18 (1953).

Girot, F.A., Fedon, R., Quenisset, J.M., and Naslain, R., *Journal of Reinforced Plastics and Composites.*, 9, pp. 456-69 (1990).

Masur, L.J., Mortensen, A., Cornie, J.A., and Flemings, M.C., *Metall. Trans. A*, 20A, pp. 2549-57 (1989).

Mortensen, A., Masur, L.J., Cornie, J.A., and Flemings, M.C. *Metall. Trans. A*, 20A, pp. 2535-47 (1989).

Nagata, S., and Matsuda, K., *Trans. Jpn. Foundarymen's Soc.*, 2, pp.616-20 (1982).